Ultra-broadband 2D electronic spectroscopy of carotenoid-bacteriochlorophyll interactions in the LH1 complex of a purple bacterium

Margherita Maiuri, Julien Réhault, Anne-Marie Carey, Kirsty Hacking, Marco Garavelli, Larry Lüer, Dario Polli , Richard J. Cogdell, and Giulio Cerullo

Citation: The Journal of Chemical Physics **142**, 212433 (2015); doi: 10.1063/1.4919056
View online: http://dx.doi.org/10.1063/1.4919056
View Table of Contents: http://scitation.aip.org/content/aip/journal/jcp/142/21?ver=pdfcov
Published by the AIP Publishing

Ultra-broadband 2D electronic spectroscopy of carotenoid-bacteriochlorophyll interactions in the LH1 complex of a purple bacterium

Margherita Maiuri,[1,2,a)] Julien Réhault,[1,a)] Anne-Marie Carey,[3] Kirsty Hacking,[3] Marco Garavelli,[4,5] Larry Lüer,[6] Dario Polli,[1] Richard J. Cogdell,[3] and Giulio Cerullo[1,b)]
[1]*CNR-IFN, Dipartimento di Fisica, Politecnico di Milano, P.zza L. da Vinci 32, Milano 20133, Italy*
[2]*Department of Chemistry, Princeton University, Washington Road, Princeton, New Jersey 08544, USA*
[3]*Glasgow Biomedical Research Centre, IBLS, University of Glasgow, 126 Place, Glasgow G12 8TA, Scotland, United Kingdom*
[4]*Dipartimento di Chimica "G. Ciamician," Università di Bologna, Via Selmi 2, IT-40126 Bologna, Italy*
[5]*CNRS, Institut de Chimie de Lyon, École Normale Supérieure de Lyon, Université de Lyon, 46 Allée d'Italie, F-69364 Lyon Cedex 07, France*
[6]*Madrid Institute for Advanced Studies, IMDEA Nanociencia, Madrid, Spain*

(Received 6 February 2015; accepted 14 April 2015; published online 28 April 2015)

We investigate the excitation energy transfer (EET) pathways in the photosynthetic light harvesting 1 (LH1) complex of purple bacterium *Rhodospirillum rubrum* with ultra-broadband two-dimensional electronic spectroscopy (2DES). We employ a 2DES apparatus in the partially collinear geometry, using a passive birefringent interferometer to generate the phase-locked pump pulse pair. This scheme easily lends itself to two-color operation, by coupling a sub-10 fs visible pulse with a sub-15-fs near-infrared pulse. This unique pulse combination allows us to simultaneously track with extremely high temporal resolution both the dynamics of the photoexcited carotenoid spirilloxanthin (Spx) in the visible range and the EET between the Spx and the B890 bacterio-chlorophyll (BChl), whose Q_x and Q_y transitions peak at 585 and 881 nm, respectively, in the near-infrared. Global analysis of the one-color and two-color 2DES maps unravels different relaxation mechanisms in the LH1 complex: (i) the initial events of the internal conversion process within the Spx, (ii) the parallel EET from the first bright state S_2 of the Spx towards the Q_x state of the B890, and (iii) the internal conversion from Q_x to Q_y within the B890. © *2015 AIP Publishing LLC.* [http://dx.doi.org/10.1063/1.4919056]

I. INTRODUCTION

Photosynthetic organisms rely on sophisticated light harvesting (LH) complexes which show an extremely high quantum yield for light-to-charge conversion (higher than 95%).[1,2] LH complexes act as natural antennae that absorb the sunlight via their main pigments—carotenoids (Cars) and chlorophylls (Chls)—and rapidly transfer the excitation energy to nearby reaction centers (RCs), where primary charge separation takes place.[3] Purple photosynthetic bacteria are ideal prototypical systems to study photosynthesis, as they rely on a small subset of pigment molecules (Cars and bacteriochlorophylls (BChls)) for LH, placed in a protein scaffold which stabilizes their relative organization.[4] Purple bacteria contain two types of LH complexes: the peripheral LH2 and the LH1/RC core complex. Both of them are large oligomers with an elementary subunit made of a heterodimer of α- and β-apoproteins bound to the Cars and BChls. Solar energy is captured by the peripheral LH2 complexes and efficiently driven towards the core-complex LH1, which contains the RC where the charge separation takes place. Sunlight absorption triggers two spectrally distinguishable parallel excitation energy transfer (EET) mechanisms: (1) a downhill EET process within and among the higher energetic BChls towards the lower ones in the near-infrared (NIR) spectral range, on a femto- to pico-second time scale,[5] and (2) a parallel sub-50 fs EET from Cars to BChls in the visible region.

Cars perform several functions in photosynthetic bacteria and plants, of which the most important one is to photoprotect the photosynthetic apparatus, by quenching both triplet excited BChl and so preventing the formation of singlet oxygen.[6] Cars also protect plants from excess illumination, by participating to the so-called non-photochemical quenching (NPQ) mechanism.[7,8] Additionally, Cars contribute to the LH process, by collecting the sunlight in the complementary blue-green spectral region and efficiently transferring it to BChls.[9] The photophysics of Cars is complicated by the fact that their first singlet excited state, S_1, has the same A_g^- symmetry as the ground state, so that the $S_0 \rightarrow S_1$ transition ($1A_g^- \rightarrow 2A_g^-$) is optically forbidden. The first optically allowed transition ($1A_g^- \rightarrow 1B_u^+$) is directed to the higher lying S_2 state of B_u^+ symmetry. Upon photoexcitation, S_2 decays non-radiatively by an internal conversion (IC) process to S_1, on the ≈300-fs time scale.[9] When Cars are incorporated in LH complexes, the $S_2 \rightarrow S_1$ IC process competes with Car → BChl EET,

[a)]M. Maiuri and J. Réhault contributed equally to this work.
[b)]Author to whom correspondence should be addressed. Electronic mail: giulio.cerullo@polimi.it.

which predominantly occurs from S_2, making the overall photoinduced dynamics significantly faster.[9,10]

Extensive spectroscopic studies on Cars, both isolated and embedded in LH complexes, have revealed a more intricate energy landscape, going beyond the three-level model and calling for the inclusion of additional dark electronic states. An intermediate state with $1B_u^-$ symmetry (named S_x) mediating the $S_2 \rightarrow S_1$ IC process has been first postulated theoretically and then experimentally demonstrated.[11–20] Recently, it has been proposed that when Cars are embedded in the LH2 complexes, S_x might play an active role in the EET towards the higher excited state Q_x of BChls.[21] Moreover, experimental evidence demonstrated the existence of another intermediate state, named S^*, involved in the IC process of the Cars, whose origin and nature are still debated.[10] It has been suggested that the S^* function is related to the NPQ role that Cars play in LH complexes, as observed in the LH1 of the purple bacterium *Rhodospirillum* (*Rsp.*) *rubrum*, where S^* is seen as the precursor of the triplet state.[22]

Disentangling the processes of IC and EET from Cars to BChls within an LH complex is a challenging task, due to the ultrafast time scale of these processes and spectral overlap of multiple features of the different molecules. The dynamics of electronic excitations in both LH2 and LH1 complexes have been extensively studied by a variety of ultrafast spectroscopy approaches, including pump-probe and fluorescence up-conversion.[23] The advent of two-dimensional electronic spectroscopy (2DES) has for the first time enabled the combination of the highest temporal and spectral resolution,[24–27] thanks to the Fourier transform analysis in the frequency domain. In a 2DES experiment, the system under study is excited by three consecutive pulses, with controllable relative delays t_1 (coherence time) and t_2 (population or waiting time). This pulse sequence builds up a macroscopic third-order nonlinear polarization in the medium that emits a field, following pulse 3 at time t_3. This field is fully measured in amplitude and phase with the help of an additional pulse, known as local oscillator (LO). Finally, by Fourier transforming with respect to t_1 and t_3 for a fixed value of the population time t_2, one derives the 2D spectrum as a function of "excitation frequency" ω_1 and "detection frequency" ω_3. 2DES thus provides a two-dimensional map that correlates excitation and detection frequencies of a system over a certain time interval (the waiting time t_2). This technique is ideally suited for multi-chromophoric systems, such as the LH complexes, in which the absorptions between states are overlapped, because it records couplings and dynamics of energy flow and allows the direct observation of coherence between electronic excitations.[28–32] Due to its unique combination of spectral and temporal resolution, 2DES has been very recently used for studying the LH complexes of purple bacteria to unveil both the electronic structure and dynamics[21,33–39] and to follow the IC dynamics of the isolated Cars.[20,40,41]

So far two experimental approaches have been successfully used to implement 2DES: the non-collinear, heterodyne-detected three-pulse photon echo[42,43] and the partially collinear pump-probe geometry.[44–46] Both approaches present advantages but also limitations and technical difficulties. In the standard implementations of non-collinear 2DES, interferometric stability is achieved by using as beam splitters (BSs) diffractive optics,[30] generating pulse pairs which impinge on the same optics and are thus intrinsically phase-locked. Alternatively, active path-length stabilization[47] can be used, at the expense of a significant complication of the experimental setup. Recently, an implementation of non-collinear 2DES that employs only conventional beam splitters and mirrors has been demonstrated.[48] The second approach to 2DES is the partially collinear pump-probe geometry,[44–46] employing two phase-locked collinear pump pulses and a non-collinear probe pulse, which is dispersed on a spectrometer. The main technical challenge of this scheme is the generation of a collinear phase-locked pump pulse pair. Michelson/Mach-Zehnder interferometers with active path-length stabilization or inline measurement of the path-length difference are commonly used in the mid-IR[49] but are difficult to extend to the visible. Alternatively, a phase-locked pulse pair can be generated by a pulse shaper, with sinusoidal spectral amplitude and phase modulation. Several solutions, including liquid crystal spatial light modulators,[50] acousto-optic modulators,[45] and acousto-optic programmable dispersive filters,[51] have been implemented.

Recently, to solve in a simple, compact and cost-effective way the problem of building a stable interferometer, we introduced a novel passive optical device, which we called TWINS[52] (Translating-Wedge-Based Identical Pulses eNcoding System). TWINS exploits the birefringence of an optical material to impose an arbitrary delay on two orthogonal polarization components by continuously varying the material thickness. It has the advantages of being inherently stable, compact, rugged, and highly reproducible. We combined TWINS with our ultra-broadband pump-probe apparatus[53] to turn it into a 2DES setup[54] with unprecedented spectral coverage, from the visible to the NIR. Thanks to the high accuracy and reproducibility of the TWINS device, the coherence time t_1 can be scanned continuously without any need of delay tracking, simplifying considerably the setup. Moreover, the design of our 2DES enables the acquisition of maps for population times (t_2) up to the picosecond time scale, to fully track the EET processes in photosynthetic bacteria. Most importantly, the two-color capability of our 2DES setup allows simultaneously relaxation dynamics of both the Car and BChls to be followed. EET between the pigments manifesting as cross peaks in 2D maps can be directly isolated and highlighted.

In this paper, we apply our recently developed 2DES apparatus, featuring simple operation and ultra-broad spectral coverage, to the study of EET processes in the LH1 complex of purple bacterium *Rsp. rubrum.* The dominating Car in this bacterium is spirilloxanthin (Spx), whose 0-0 $S_0 \rightarrow S_2$ transition peaks at 540 nm, while the BChl is named B890 (actually 881) due to its Q_y band peaking at 881 nm (the higher energy Q_x band peaks at 585 nm). Thanks to our capability of generating ultra-broadband pulses spanning from the visible to NIR spectral range, we can fully cover the main ground state absorption peaks of both the Spx and the B890. By exciting in the visible range and detecting over both visible and NIR ranges, we can follow all the photoinduced processes, namely, (i) the Car internal conversion, (ii) the BChl $Q_x \rightarrow Q_y$ internal conversion, and (iii) the Car $\rightarrow$ BChl EET process. We model our experimental data by a global analysis obtaining

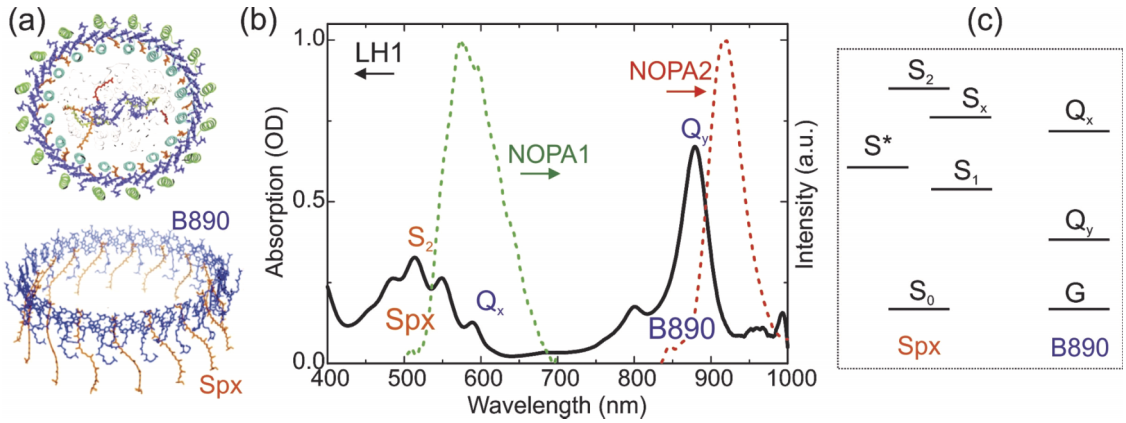

FIG. 1. (a) Top view of the arrangement of the LH1 complex and supramolecular architecture of the BChl B890 (purple) and the Car Spx (orange); (b) absorption spectrum of LH1 complex extracted from *Rsp. rubrum* (black line) and pulse spectra used in the 2DES experiments in the visible (NOPA1, green line) and near-IR (NOPA2, red line) wavelength regions; (c) energy level scheme of the Spx and the B890.

the two-dimensional evolution associated spectra (2D-EAS) describing the different steps of the photoinduced dynamics.

II. EXPERIMENTAL

A. Sample preparation

Although the crystallographic structure of LH2 complex has been known for 20 years,[55] the detailed structure of a LH1–RC has been only recently reported for the *Thermochromatium tepidum* purple bacteria.[56] In this species, unlike the case of *Rhodopseudomonas palustris* that has a gap in the LH1 ring, the RC is completely surrounded by the LH1 ring of 16 αβ-subunits. The supramolecular architecture of the pigments in LH1 is characterized by an elliptical array of 32 BChl molecules and 16 Cars arranged in a tightly stacked ring (Fig. 1(a)).[56] The LH1 complex from *Rsp. rubrum* contains one type of carotenoid, Spx, and one type of BChl, named B890 due to its main optical absorption (Figs. 1(b) and 1(c)).

Rsp. rubrum S1 cells were grown anaerobically in the light and chromatophore membranes prepared as previously described[57] with the modification that the chromatophores were pelleted by centrifugation for one hour at 208 000 g. The LH1/RC complex was prepared as described by Nakagawa *et al.*[58] with the exception that the β-dodecyl maltoside (DDM) was substituted for lauryldimethylamine n-oxide (LDAO). In brief, the chromatophores at an optical density (OD) of 50 at 890 nm were solubilised with 2% (w/v) DDM, and the LH1/RC complex was initially fractionated using sucrose density centrifugation with the following sucrose concentrations 0.8 M, 1.0 M, 1.2 M, 1.4 M, and 1.6 M, in 20 mM Tris-HCl, 0.02% (w/v) DDM. The LH1/RC fraction was removed from the gradients and further purified by anion exchange chromatography on Whatman DE52 cellulose resin. The LH1/RC complex was then finally purified by size exclusion chromatography on a Superdex G200 (GE Healthcare) column.

B. Ultrabroadband 2DES setup

The 2DES setup used in these measurements is represented in Fig. 2 and has been described in detail in our recent paper.[59] It uses the partially collinear pump-probe geometry,[49,60] which is easy to implement into an existing pump-probe setup and which makes it particularly suitable for 2-color measurements. The working principle of TWINS is explained in the supplementary material[61] (Fig. S1) and has been described in details elsewhere.[52,59] The system starts with a commercially amplified Ti:sapphire laser system (Libra, Coherent) delivering 4-mJ, 100-fs pulses at 800 nm, and 1-kHz repetition rate. A portion of the laser with 300 μJ energy pumps two synchronized non-collinear optical amplifiers (NOPAs) which feed the 2DES setup. The first NOPA (NOPA1) delivers visible pulses with a spectrum spanning from 520 nm to 700 nm, compressed to sub-10-fs duration by multiple bounces

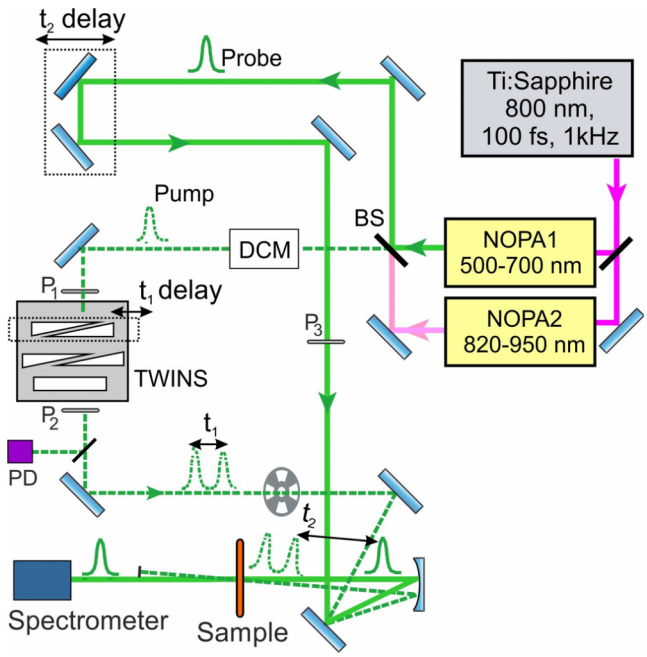

FIG. 2. Scheme of the experimental 2DES apparatus in the pump-probe configuration. TWINS: interferometer for pulse pair generation; BS: beam splitter; DCM: double chirped mirror; PD: photodiode; P: polarizer. The BS necessary for one-color measurements with the visible NOPA (NOPA1) is replaced with a mirror to run two-color 2D measurements combining the visible NOPA1 with the NIR NOPA (NOPA2).

on custom-designed double-chirped mirrors (DCMs). The second NOPA (NOPA2) delivers NIR pulses with a spectrum spanning between 850 nm and 1100 nm, compressed to sub-15-fs duration by a double pass in a Brewster-cut fused silica prism pair. In degenerate 2DES, pump and probe are separated by a beam splitter, while in the two-colour configuration, the two beams come from different NOPAs. The pair of pump pulses is generated by the TWINS setup, while the probe pulse is delayed by t_2 via a conventional translation stage. There are no restrictions on the maximum t_2 delay, which in the current setup is ≈100 ps and only limited by the excursion of the t_2 translation stage.

Part of the pump beam is split off and sent to a photodiode to monitor the interferogram of the pump pulse pair, which is used to determine time zero and properly phase the 2DES spectra. The additional dispersion introduced by the TWINS on the pump pulse pair is compensated by a suitable number of bounces on a pair of DCMs, and spectral phase correction is verified using a SEA-TADPOLE setup.[62] Pump and probe pulses are non-collinearly focused on the sample, and the transmitted probe light is dispersed on a spectrometer.[53]

Besides the ease of use, noticeable advantages of this configuration are the speed of acquisition and the repeatability. By using continuous scanning of the t_1 delay with the TWINS, we are able to measure a 2DES spectrum in less than 10 s, depending on the t_1 scan length. The setup does not require any type of delay tracking, since we exploit the constant speed of the translation stage during the acquisition and the demultiplication effect of the wedges to perform a reliable Fourier transform along t_1.

C. Global analysis of the 2DES maps

A global kinetic analysis of the 2DES maps at all t_2 times has been performed by non-linear optimization, minimizing the total error squared E between the calculated and the experimental 2DES maps: $E = \sum_{\lambda_{exc}} \left(A_{exp}^{\lambda_{exc}}(\lambda_{det}, t_2) - A_{calc}^{\lambda_{exc}}(\lambda_{det}, t_2) \right)^2$, where $A_{exp}^{\lambda_{exc}}(\lambda_{det}, t_2)$ is a matrix of the measured differential transmission (ΔT/T) values as function of the detection wavelength λ_{det} and t_2 is a time for a specific excitation wavelength λ_{exc}. The calculated matrix is obtained using Lambert-Beer's law, for small values of A, in matrix notation, $A_{calc}^{\lambda_{exc}}(\lambda_{det}, t_2) = \sigma^{\lambda_{exc}}(\lambda_{det}, i) \times c(i, t_2)$. Here, $c(i, t_2)$ is the matrix of time-resolved concentrations of species i for all t_2 times, which is obtained by numerical integration of a set of rate equations for an unbranched, unidirectional reaction scheme (only first state is created by pump, only last state relaxes to ground state) of first order processes, using standard ordinary differential equation solvers. The associated matrix of characteristic spectra $\sigma^{\lambda_{exc}}(\lambda_{det}, i)$ for each component i is found for each value of the excitation wavelength during each iteration of the minimization of E. Convergence is reached by variation of the rate constants involved in the sequential reaction scheme. The analysis is performed by a problem solving environment, written in-house, that allows the design of specific weight functions along all directions in order to adjust the emphasis of the fitting according to the density of t_2 values or the amount of measurement noise. The result of the global analysis is a set of rate constants $k_1, k_2, \ldots, k_i$, reflecting the lifetimes of the states i in the sequential model, and their associated characteristic transient spectra for each value of the excitation wavelength, $\sigma^{\lambda_{exc}}(\lambda_{det}, i)$, that can be re-composed into a set of two-dimensional evolution associated spectra, $2D - EASi(\lambda_{exc}, \lambda_{det})$.[63] As the vertical axis of the original 2DES maps has not been normalised to uniform excitation intensity, it follows that vertical sections through the resulting 2D-EAS maps yield excitation spectra multiplied by the spectral intensity distribution of the pump. For the global fitting procedure, this is equivalent to giving additional weight to those spectral regions where the excitation pulse has higher intensity.

If the photophysical evolution of the system, as in the present case, is not purely sequential but comprises parallel and possibly backward reactions, then the 2D-EAS are linear combinations of the two-dimensional species associated spectra (2D-SAS) that would correspond to pure photophysical states. The weight of the different 2D-SAS in each 2D-EAS can in principle be obtained by spectral decomposition techniques. For the purposes of this work, the information contained in the 2D-EAS is however sufficient to clearly demonstrate coherent couplings between different excited states as well as ultrafast branching of relaxation paths.

III. RESULTS AND DISCUSSION

A. Degenerate 2DES

Figure 3 shows experimental 2DES maps for the LH1 complex of *Rsp. rubrum* acquired in the degenerate configuration at different population (t_2) time delays, as indicated in each panel. The maps presented in Fig. 3 (as well as those in Fig. 4) are not normalized to the pump pulse spectrum. The visible NOPA (NOPA1 in Fig. 1(b)) was tuned in order to cover both the 0-0 vibronic replica of the S_0–S_2 absorption of the Car (540 nm) and the Q_x singlet excited state of the B890 BChl (585 nm). At very early times (t_2 = 0 fs, top left panel in Fig. 3), the 2D map is dominated by features with positive ΔT/T signal (red portion of the palette, solid contour lines). On the diagonal (drawn as gray dashed line), we find the photobleaching (PB) of the 0-0 vibronic transition of S_2; it is elongated towards 560 nm where, in a similar LH2 complex, the presence of PB from the S_x state has been proposed.[20] Our data support this picture by showing positive cross peaks between S_2 and S_x in the upper as well as in the lower triangle. The positive diagonal peak at 585 nm is assigned to resonant pumping of the Q_x band of B890. As long as the B890 population has not yet undergone IC from Q_x to Q_y, we expect to observe on the diagonal a superposition of PB and stimulated emission (SE) from Q_x. In the lower triangle, there is a positive band that could be assigned to a cross peak between Q_x and S_2. However, its shape is horizontally elongated towards the red up to 610 nm detection wavelength, which is not the case for the diagonal peak of Q_x. We therefore assign the portion of the off-diagonal peak at longer detection wavelengths to SE from S_2 to S_0. Besides the positive bands, we only observe two very faint PA bands (negative ΔT/T signal, blue portion of the palette, dashed contour lines) pumping at 545 nm and probing

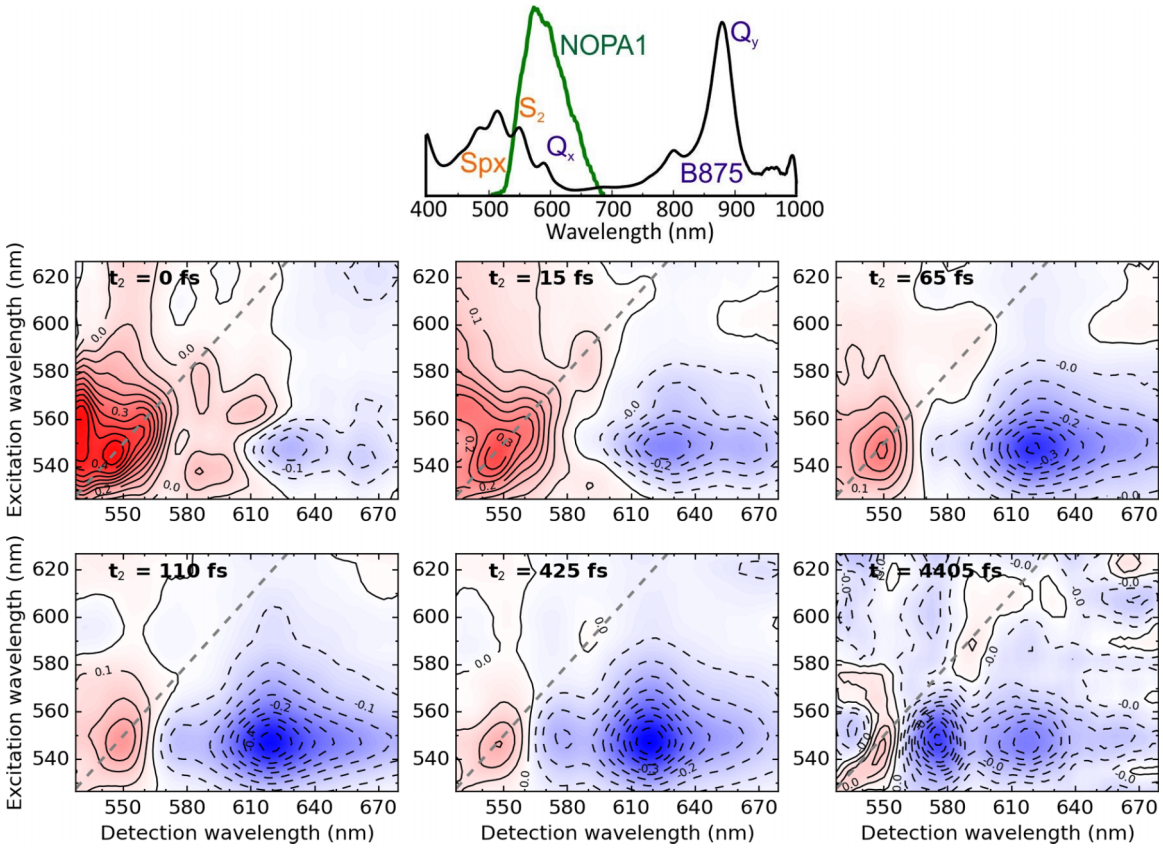

FIG. 3. Degenerate 2DES maps of the LH1 complex from *Rsp. rubrum*, for different population times t_2, following excitation by a sub-10-fs visible pulse, resonant with the $S_0 \rightarrow S_2$ transition of the Car and the Q_x transition of the BChl. All panels have a color code ranging from $\Delta T/T = -0.5$ (blue) to +0.5 (red), except the very last map, which has been scaled from −0.15 to +0.15. The absorption spectrum of the LH1 complex and the spectrum of NOPA1 are reported in the upper panel.

at 630 and 660 nm. These bands are associated with the hot S_1 state, which is created in small amounts already during the temporal overlap of the pulses around $t_2 = 0$ delay.

At $t_2 = 15$ fs, which is close to our effective temporal resolution, we find that the SE(S_2) feature has become much weaker, but the S_x-related features are still present. Since also PA(S_1) has not increased substantially from 0 to 15 fs, this is an indication that S_2 does not feed S_1 directly but populates S_x first, with most of the $S_2 \rightarrow S_x$ IC dynamics occurring on the 10-fs time scale, in agreement with previous findings.[14–17,20] At $t_2 = 65$ fs, both SE(S_2) and the S_x-related features have completely disappeared, leaving PB(S_2) as the most important diagonal feature. At the same excitation wavelength of 545 nm, a strong PA at 630 nm detection wavelength, with a shoulder at 660 nm, indicates that most of the population that resided formerly in S_2 and S_x now has internally converted into a hot S_1 state. Note that in molecular systems like Cars and BChls, any photoexcitation, irrespective of its type, in general bleaches all ground state transitions at the same relative intensity; this explains the observation of a leftover PB(S_2) while population has converted to S_1. Note also that the diagonal peak of Q_x has become less pronounced after 65 fs, indicating that population in the B890 moiety, which was resonantly created on Q_x after pumping at 585 nm, has started the IC process to Q_y, reducing the SE contribution to the positive signal on the diagonal. After IC, SE is expected on Q_y instead of Q_x, which will be shown to be the case in the two-color 2DES data (see next paragraph). We also see the start of the formation of a new cross-peak, with PA peaking at 575 nm, assigned to the S^* state.

At $t_2 = 110$ fs, we observe a blue shift of the PA band from 630 to 620 nm and a relative decrease of the shoulder at 660 nm, both associated with vibrational cooling of the hot S_1 state. At 4 ps delay, the dominant PA band becomes the S^* state (at 570-nm detection wavelength), because its lifetime is longer than PA(S_1) (which decays on the picosecond time scale).[22]

B. Two-colour 2DES

Figure 4 shows the two-colour 2DES maps in which we excite the LH1 complex with the visible NOPA (NOPA1), in resonance with the S_2 state of the Car and the Q_x of the B890, and detect the photo-induced dynamics of the Q_y band of B890 in the NIR spectral region (NOPA2 in Fig. 1(b)). At very early times ($t_2 = 0$ fs, top left panel in Fig. 4), we observe two positive cross peaks at 875 nm detection wavelength that appear at the excitation wavelengths of 545 and 585 nm, corresponding to resonances of S_2 and Q_x. The center wavelength of the positive bands at 875 nm identifies these features as pure PB contributions from Q_y, showing that at these early t_2 times, the population is still entirely on Q_x and the optical probes which are specific for population in Q_y, namely, PA on the short wavelength side and SE on the long wavelength side, are still absent. On the contrary, we observe

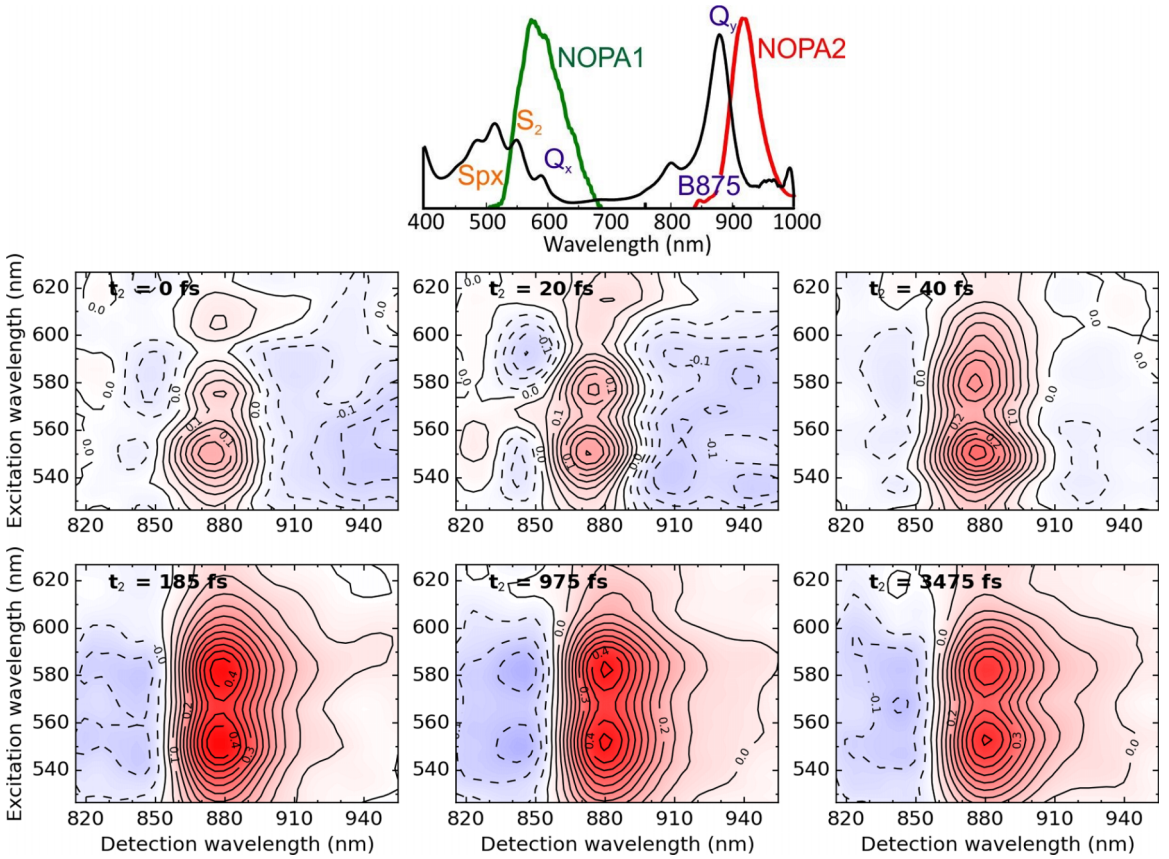

FIG. 4. Experimental 2DES maps as a function of excitation and detection wavelengths of LH1 complex obtained for the two-color experiment at different t_2 delays. All panels have a color code ranging from $\Delta T/T = -0.5$ (blue) to +0.5 (red). The absorption spectrum of the LH1 complex and the spectra of NOPA1 and NOPA2 are reported in the upper panel.

the presence of an intense negative peak around 940 nm, which is a well-known feature of the Car and is associated with PA from S_2 to higher lying states.[18] This signal extends to longer excitation wavelengths where there is a weak tail of the ground state absorption spectrum of the Car. At t = 20 fs, very short time after the end of the pump pulse, we observe a strong increase of the PB(Q_x) features, while PA(S_2) does not increase significantly, an indication that loss towards S_x partially occurs already during the excitation pulse which continuously creates it. At t_2 = 40 fs, the PA contribution from the Car has nearly disappeared. On the 100-fs time scale, the further evolution of the 2DES maps in Fig. 4 consists in the growth of the positive cross peaks at 875 nm and the appearance of two PA peaks on the short wavelength side, around 845 nm. Both the features at 875 and 845 nm are specific optical probes for population on Q_y, showing that both the Car → BChl EET and the IC from Q_x to Q_y are occurring at this time scale. Additionally, an apparent red shift of the main PB band from 875 to 880 nm is observed on the same time scale. This apparent red shift is caused by superposition with the PA at 840 nm, showing the strongly delocalized nature of the Q_y exciton.[64]

C. Global analysis of the 2D maps

We performed a global analysis of the time-resolved 2D maps, using an unbranched unidirectional model (for the definition and further details, see Sec. II C). The fitted 2D maps are reported in the supplementary material[61] (Figs. S2 and S3). The excellent agreement with the experimental maps testifies the quality of our data and the appropriateness of the fitting model employed. Figure 5 shows the five evolutionary states (2D-EAS) that reproduce the 2DES maps in the visible region, together with their exponential lifetimes (i.e., the inverse of the rate constants k_i). Due to the presence of parallel and possibly also backward photophysical processes, these 2D-EAS should be understood as superpositions of pure photophysical states with relative spectral weights varying from one 2D-EAS to the next one. The lifetime of the first evolutionary state, 2D-EAS1, has been fixed to 10 fs in the global fitting and therefore summarizes the effects occurring on the ultrafast time scale comparable with our temporal resolution: resonant photoexcitation, coherent effects, and ultrafast transfer events requiring coherence. In this sense, 2D-EAS1 show the presence of S_2 (via SE at 580-610 nm detection wavelength), S_x (via PB on the diagonal at 560 nm and S_2−S_x cross peaks) and Q_x (via PB and SE at 585 nm on the diagonal). The fact that very little PA(S_1) is found in 2D-EAS1 confirms that there is sub-10 fs IC from S_2 into S_x but not strongly into S_1. The next evolutionary state, 2D-EAS2, is found to have a lifetime of 44 fs. The evolution from 2D-EAS2 to 2D-EAS3 consists in the loss of S_x and the build-up of both hot S_1 (at 620 nm detection wavelength) and S^* (at 580 nm detection wavelength), showing that the overall S_2/S_x deactivation proceeds with a 44 fs time constant,

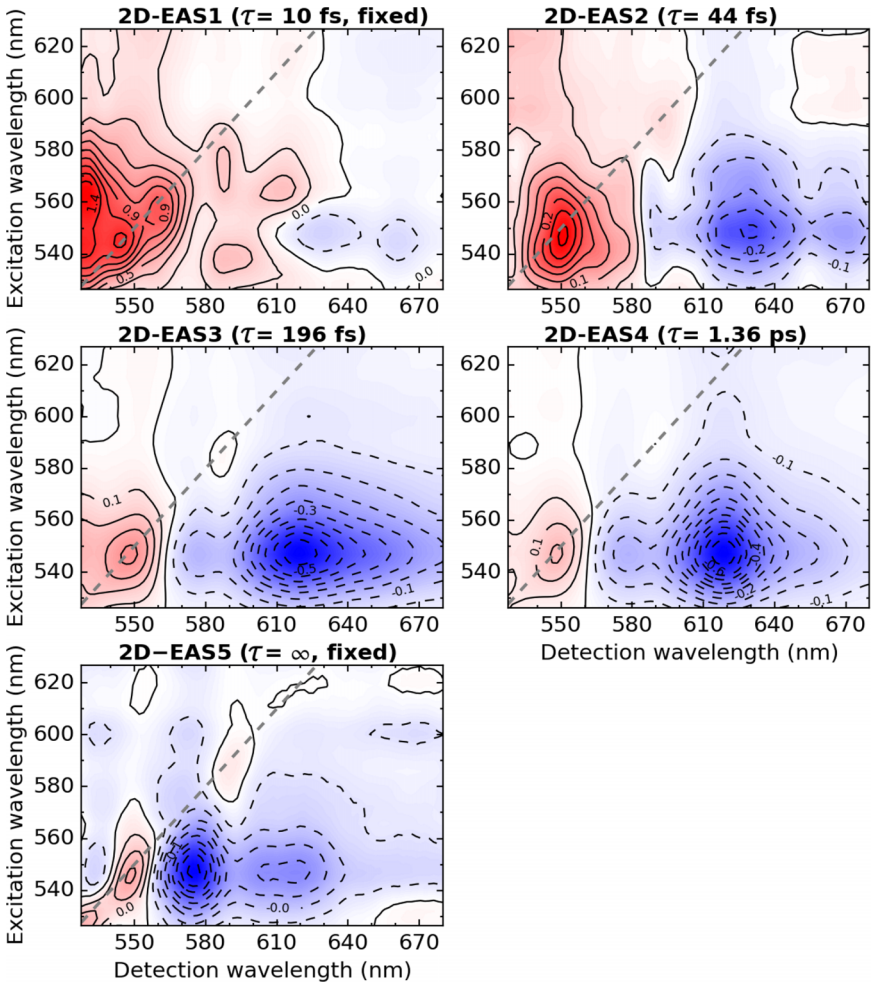

FIG. 5. 2D-EAS from a global fit of the 2D maps in the visible probe spectral region. The 2D-EAS have a lifetime of $\tau_1 = 10$ fs (fixed), $\tau_2 = 44$ fs, $\tau_3 = 196$ fs, $\tau_4 = 1.36$ ps, and $\tau_5 =$ infinite (fixed), respectively.

yielding hot S_1, S^* and—as Fig. 4 shows—also Q_x. This dynamics should be compared to the one of isolated Spx in solution, which has been characterized by pump-probe spectroscopy;[65] in that case, the build-up time constant of hot S1 was found to be ≈100 fs. The significant shortening, by a factor of more than 2, within the LH complex is consistent with the opening of an additional relaxation channel for S_2/S_x, besides IC to S_1: EET to the BChl. The transition from

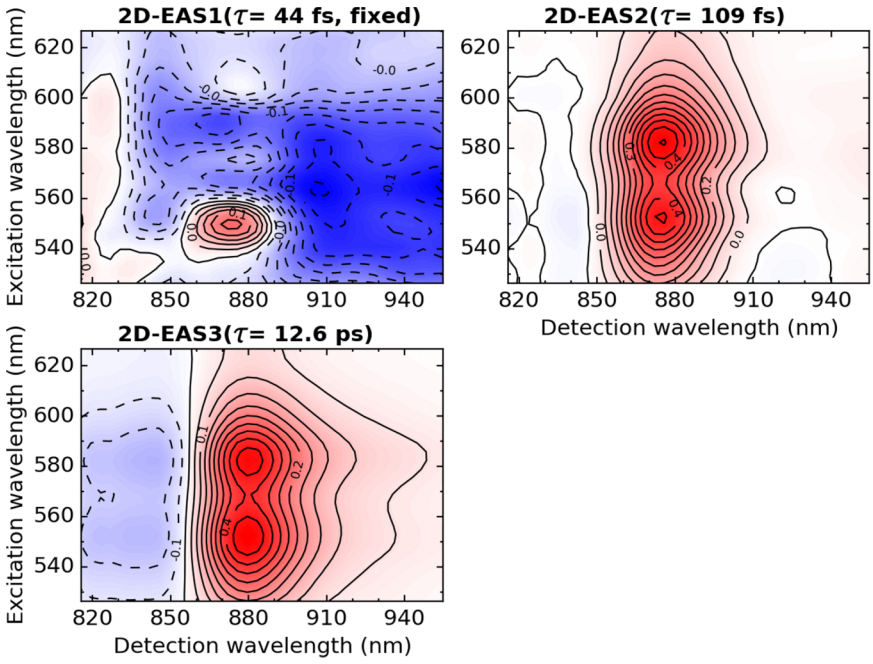

FIG. 6. 2D-EAS from a global fit of the 2D maps in the near infrared probe spectral region. The lifetimes of the 2D-EAS are $\tau_1 = 44$ fs (fixed), $\tau_2 = 109$ fs, $\tau_3 = 12.6$ ps.

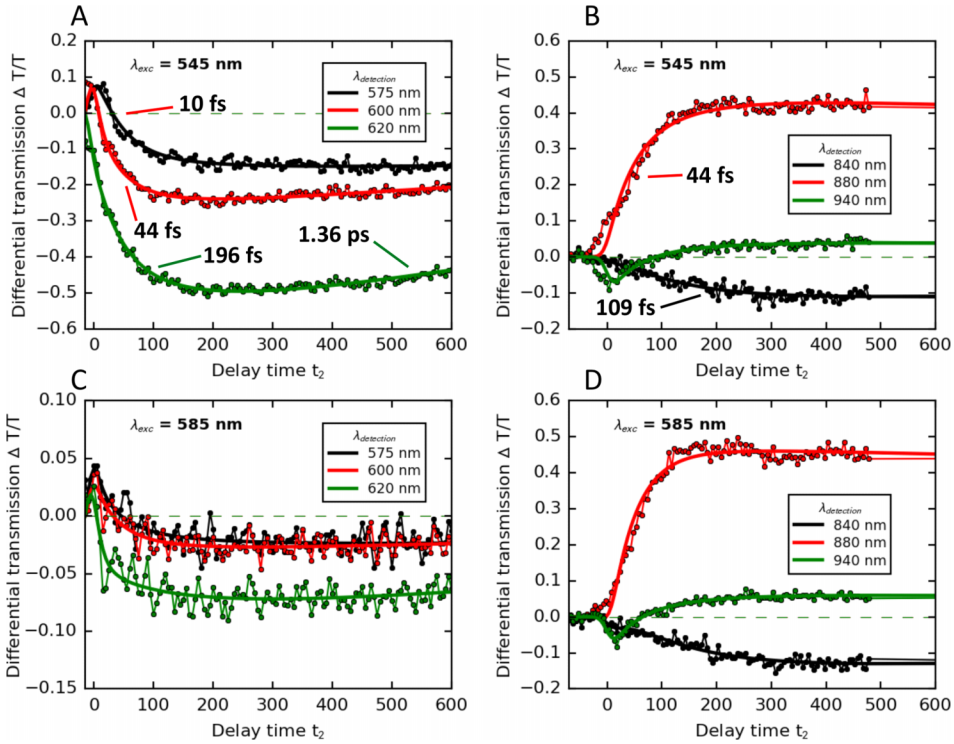

FIG. 7. Dynamics at selected excitation and detection wavelengths, as indicated (points connected by thin curves). Each data point corresponds to a single 2DES map, from which the ΔT/T value at the given excitation and detection wavelength was extracted. Thick curves are from the global fit that produced the 2D-EAS in Figs. 5 and 6 for panels (a) and (b) and panels (c) and (d), respectively. Time constants annotated to decay traces in A and B refer to the most prominent decay components with respect to global fitting.

2D-EAS3 to 2D-EAS4 (196 fs time constant) essentially reflects hot S_1 thermalization,[65] while the transition from 2D-EAS4 to 2D-EAS5 (1.36 ps time constant[65]) refers to loss of S_1. The final 2D-EAS5 show S^* as dominant photoexcitation. The minor presence of S_1 in 2D-EAS5 can be explained by contribution of non-exponential channels to the relaxation of S_1.

In Fig. 6, we show the 2D-EAS for the 2D maps in the NIR, with the associated lifetimes. We first tried to optimize all three rate constants independently; however, we observed a strong cross talk between k_1 and k_2. We found that there is strong interdependence between the value of k_1 and the relative amplitude of the 2D-EAS features so that a reliable value for the fastest rate constant could not be obtained from the fits of the NIR part alone. Therefore, we fixed the lifetime of 2D-EAS1 to $(k_1)^{-1}$ = 44 fs, corresponding to the S_2/S_x lifetime obtained from fitting the visible part in Fig. 5. Obviously, this choice, while neutral to the quality of the fits (see the supplementary material[61]), has influence on the shape of the resulting 2D-EAS, which in turn fully confirms the photophysical picture developed from the global fits in the visible spectral region. Thus, 2D-EAS1 show strong PA centred at 910 nm, in which weak positive bands of PB(Q_y) are immersed. The PA is associated with S_2/S_x, while the presence of PB(Q_y) at a pumping wavelength of 585 nm is caused by a resonant creation of population on Q_x, under the notion that population on any excited state of a molecular system bleaches the entire ground state absorption spectrum (both Q_x and Q_y in this case). The origin of PB(Q_y) after pumping S_2 might be an ultrafast S_2-Q_x EET, although further studies are necessary to prove this mechanism. The second evolutionary spectrum, 2D-EAS2, is a very pure one, showing only PB(Q_y). The complete absence of any PA in 2D-EAS2 confirms that the lifetime of 44 fs which we assumed for 2D-EAS1 indeed refers to the lifetime of the S_2/S_x states as concluded from the global fit of the visible region. On the other hand, also the typical features of the Q_y exciton, namely, SE on the red side of PB(Q_y) and PA on its blue side, are completely absent in 2D-EAS2. This evolutionary state is therefore that of a single photoexcitation, namely, the Q_x state. This observation unambiguously shows that ET from S_2/S_x creates population in the Q_x manifold, as predicted by Ostrumov *et al.* from single color 2DES in similar systems.[20,21] Finally, 2D-EAS3 show the presence of SE, clearly evidenced by the fact that it extends as far as 950 nm where Q_y does not have any ground state absorption. It also shows PA on the short wavelength side, which is so strongly superposed with PB(Q_y) that it causes an apparent red shift of the PB maximum from 875 to 880 nm. The presence of a PA band which is only slightly blue shifted against the parent PB band is well known for highly delocalized circular excitons of Q_y states.[66] 2D-EAS3 are therefore also identified as a pure photoexcitation, namely, thermalized and strongly delocalized Q_y excitons. Since both 2D-EAS 2 and 2D-EAS3 are shown to be pure states, the lifetime of 2D-EAS2, 109 fs, is directly associated with the internal conversion from Q_x to Q_y, which is here clearly resolved for the first time.

Our conclusions from the global analysis are confirmed by presenting selected time traces in Fig. 7. Panel (a)[(c)] shows dynamics at three different detection wavelengths in the visible after exciting at 545[585] nm. At detection wavelengths where SE(S_2) has significant oscillator strength (575 and 600 nm, corresponding to black and red curve/dots, respectively), we find a very sharp drop of the initially positive signal, associated with the ultrashort lifetime of the S2 state. In contrast, the pure build-up of PA(S_1), measured at 620 nm (green curve/dots in panel (a)), does not show such an ultrafast component, being instead dominated by the 44 fs build-up time as obtained for

2D-EAS2 in Fig. 5, followed by a slower build-up component at 196 fs, associated with hot S_1 thermalization, adding oscillator strength from the shoulder at 660 nm detection wavelength to the band maximum at 620 nm. From the absence of the ultrafast component in the build-up of the PA(S_1) band, we thus learn that population of S_1 is therefore only created once the ultrafast conversion from S_2 to S_x has been accomplished; this is in agreement with our conclusions from 2D-EADS 0-2 in Fig. 5. Finally, note the slight decrease of the dynamics at PA(S_1), at 600 and 620 nm, while the S^* band at 575 nm is still slightly increasing (black curve/dots in panel (a)).

Panel (b)[(d)] shows dynamics in the NIR detection wavelength region after exciting at 545[585] nm. At a probe wavelength of 880 nm (red curve/dots), we follow the build-up of PB(Q_y) (caused by EET from Car into B890), superposed with the build-up of SE and PA, both arising from $Q_x \rightarrow Q_y$ IC. In order to disentangle these contributions to the maximum of the positive band at 880 nm, we also present the dynamics at 840 nm and at 940 nm detection wavelengths. It is evident that the PA at 840 nm builds up symmetrically with the SE at 940 nm (once the small initial contribution of PA(S_2) has disappeared). Compared to these isolated optical probes for population on Q_y, the dynamics at 880 nm probes both the Q_x (through the PB of Q_y) and the Q_y populations. The rise of the 880-nm in panel (d) is faster than in panel (b), consistent with a direct $Q_x \rightarrow Q_y$ IC process as compared to the two-step Car $\rightarrow$ BChl EET followed by $Q_x \rightarrow Q_y$ IC. We finally note that most of the time traces in Fig. 7 display long-lived oscillatory features, which are assigned to impulsively excited ground-state vibrational modes of the Car backbone.

IV. CONCLUSIONS

In this paper, we have presented the first example of ultra-broadband 2DES addressing the interaction between Cars and BChls in a LH complex of a purple bacterium: the LH1 complex of *Rsp. rubrum*. Purple bacteria are ideal model systems for the study of the mechanisms of photosynthesis, since Cars and BChls have well separated absorption bands: the Cars peak in the visible and the BChls in the NIR. On the other hand, the study of Car/BChl interactions by 2DES calls for an ultrabroad bandwidth, which challenges most of current 2DES implementations. Here, we show that our recently introduced 2DES setup, working in the partially collinear pump-probe geometry and based on a passive birefringent interferometer (the TWINS device), ideally lends itself two 2DES in a two-colour configuration and allows to follow simultaneously the relaxation dynamics of both the Car and BChl and to track IC within the pigments and EET between the pigments. The sequence of 2DES spectra, which are modeled by a 2D-EAS analysis, enables all photoinduced processes to be disentangled, namely, (i) the $S_2 \rightarrow S_1$ IC process in the Car, which we find to be mediated by the S_x state, (ii) formation of the long-lived S^* state in the Car, (iii) EET from the S_2 state of the Car to the Q_x state of the BChl, which is followed by $Q_x \rightarrow Q_y$ IC, and (iv) direct $Q_x \rightarrow Q_y$ IC in the BChl. In the future, it will be interesting to extend such ultra-broadband 2DES studies to even more complicated systems, such as membranes of photosynthetic bacteria containing both LH2 and LH1 complexes, or the photosystems of higher plants.

ACKNOWLEDGMENTS

M.G. and G.C. acknowledge support by the European Research Council Advanced Grant STRATUS (ERC-2011-AdG No. 291198). J.R. thanks the Swiss National Science Foundation for financial support (Fellowship PBZHP2_143444). L.L. acknowledges support from the Spanish Ministry of Economy and Competitiveness (Project CONMOL) and from the EU via the COFUND program AMAROUT. A.M.C. and R.J.C. were supported by the Photosynthetic Antenna Research Centre (PARC), an Energy Frontier Research Centre funded by the DOE, Office of Science, Office of Basic Energy Sciences under Award No. DE-SC 0001035. K.H. was supported by an EPSRC studentship.

[1]R. E. Blankenship, *Molecular Mechanisms of Photosynthesis* (Blackwell Science, Oxford, UK, 2002).
[2]R. Blankenship *et al.*, Science **332**, 805 (2011).
[3]R. J. Cogdell, A. Gall, and J. Kohler, Q. Rev. Biophys. **39**, 227 (2006).
[4]R. J. Cogdell *et al.*, J. Bacteriol. **181**, 3869 (1999), pdf available at http://jb.asm.org/content/181/13/3869.full.pdf+html.
[5]V. Sundstrom *et al.*, J. Phys. Chem. B **103**, 2327 (1999).
[6]M. Griffith, W. R. Sistrom, G. Cohen-Bazire, and R. Y. Stanier, Nature **176**, 1211 (1955).
[7]A. V. Ruban, R. Berera, C. Ilioaia, I. H. M. van Stokkum, J. T. M. Kennis, A. A. Pascal, H. van Amerongen, B. Robert, P. Horton, and R. van Grondelle, Nature **450**, 575 (2007).
[8]T. K. Ahn, T. J. Avenson, M. Ballottari, Y.-C. Cheng, K. K. Niyogi, R. Bassi, and G. R. Fleming, Science **320**, 794 (2008).
[9]T. Polívka and V. Sundström, Chem. Rev. **104**, 2021 (2004).
[10]T. Polívka and V. Sundström, Chem. Phys. Lett. **477**, 1 (2009).
[11]P. Tavan and K. Schulten, Phys. Rev. B **36**, 4337 (1987).
[12]T. Sashima, Y. Koyama, T. Yamada, and H. Hashimoto, J. Phys. Chem. B **104**, 5011 (2000).
[13]K. Furuichi, T. Sashima, and Y. Koyama, Chem. Phys. Lett. **356**, 547 (2002).
[14]G. Cerullo, D. Polli, G. Lanzani, S. De Silvestri, H. Hashimoto, and R. J. Cogdell, Science **298**, 2395 (2002).
[15]D. Polli, G. Cerullo, G. Lanzani, S. De Silvestri, K. Yanagi, H. Hashimoto, and R. J. Cogdell, Phys. Rev. Lett. **93**, 163002 (2004).
[16]E. Ostroumov, M. G. Müller, C. M. Marian, M. Kleinschmidt, and A. R. Holzwarth, Phys. Rev. Lett. **103**, 108302 (2009).
[17]M. Maiuri, D. Polli, D. Brida, L. Lüer, A. M. LaFountain, M. Fuciman, R. J. Cogdell, H. A. Frank, and G. Cerullo, Phys. Chem. Chem. Phys. **14**, 6312 (2012).
[18]Y. Koyama, F. S. Rondonuwu, R. Fujii, and Y. Watanabe, Biopolymers **74**, 2 (2004).
[19]F. S. Rondonuwu, K. Yokoyama, R. Fujii, Y. Koyama, R. J. Cogdell, and Y. Watanabe, Chem. Phys. Lett. **390**, 314 (2004).
[20]E. E. Ostroumov, R. M. Mulvaney, R. J. Cogdell, and G. D. Scholes, Science **340**, 52 (2013).
[21]E. E. Ostroumov, R. M. Mulvaney, J. M. Anna, R. J. Cogdell, and G. D. Scholes, J. Phys. Chem. B **117**, 11349 (2013).
[22]C. C. Gradinaru, J. T. M. Kennis, E. Papagiannakis, I. H. M. van Stokkum, R. J. Cogdell, G. R. Fleming, R. A. Niederman, and R. van Grondelle, Proc. Natl. Acad. Sci. U. S. A. **98**, 2364 (2001).
[23]R. van Grondelle and V. I. Novoderezhkin, Phys. Chem. Chem. Phys. **8**, 793 (2006).
[24]D. M. Jonas, Science **300**, 1515 (2003).
[25]D. M. Jonas, Annu. Rev. Phys. Chem. **54**, 425 (2003).
[26]J. P. Ogilvie and K. J. Kubarych, in *Advances in Atomic, Molecular, and Optical Physics*, edited by P. R. Berman, C. C. Lin, and E. Arimondo (Academic Press, 2009), Vol. 57.
[27]A. M. Brańczyk, D. B. Turner, and G. D. Scholes, Ann. Phys. **526**, 31 (2014).
[28]Y.-C. Cheng and G. R. Fleming, J. Phys. Chem. A **112**, 4254 (2008).
[29]M. Cho, T. Brixner, I. V. Stiopkin, H. M. Vaswani, and G. R. Fleming, J. Chin. Chem. Soc. **53**, 15 (2006).
[30]T. Brixner, J. Stenger, H. M. Vaswani, M. Cho, R. E. Blankenship *et al.*, Nature **434**, 625 (2005).

[31]A. Ishizaki and G. R. Fleming, J. Phys. Chem. B **115**, 6227 (2011).
[32]A. Ishizaki and G. R. Fleming, Annu. Rev. Condens. Matter Phys. **3**, 333 (2012).
[33]E. Harel, P. D. Long, and G. S. Engel, Opt. Lett. **36**, 1665 (2011).
[34]A. F. Fidler, V. P. Singh, P. D. Long, P. D. Dahlberg, and G. S. Engel, J. Chem. Phys. **139**, 155101 (2013).
[35]A. F. Fidler, V. P. Singh, P. D. Long, P. D. Dahlberg, and G. S. Engel, Nat. Commun. **5**, 3286 (2014).
[36]G. S. Schlau-Cohen, T. R. Calhoun, N. S. Ginsberg, M. Ballottari, R. Bassi, and G. R. Fleming, Proc. Natl. Acad. Sci. U. S. A. **107**, 13276 (2010).
[37]E. L. Read, G. S. Schlau-Cohen, G. S. Engel, T. Georgiou, M. Z. Papiz, and G. R. Fleming, J. Phys. Chem. B **113**, 6495 (2009).
[38]D. Zigmantas, E. L. Read, T. Mancàl, T. Brixner, A. T. Gardiner, R. J. Cogdell, and G. R. Fleming, Proc. Natl. Acad. Sci. U. S. A. **103**, 12672 (2006).
[39]G. S. Schlau-Cohen, E. De Re, R. J. Cogdell, and G. R. Fleming, J. Phys. Chem. Lett. **3**, 2487 (2012).
[40]N. Christensson, F. Milota, A. Nemeth, J. Sperling, H. F. Kauffmann, T. Pullerits, and J. Hauer, J. Phys. Chem. B **113**, 16409 (2009).
[41]T. R. Calhoun, J. A. Davis, M. W. Graham, and G. R. Fleming, Chem. Phys. Lett. **523**, 1 (2012).
[42]M. L. Cowan, J. P. Ogilvie, and R. J. D. Miller, Chem. Phys. Lett. **386**, 184 (2004).
[43]T. Brixner, I. V. Stiopkin, and G. R. Fleming, Opt. Lett. **29**, 884 (2004).
[44]L. P. DeFlores, R. A. Nicodemus, and A. Tokmakoff, Opt. Lett. **32**, 2966 (2007).
[45]S.-H. Shim, D. B. Strasfeld, Y. L. Ling, and M. T. Zanni, Proc. Natl. Acad. Sci. U. S. A. **104**, 14197 (2007).
[46]E. M. Grumstrup, S.-H. Shim, M. A. Montgomery, N. H. Damrauer, and M. T. Zanni, Opt. Express **15**, 16681 (2007).
[47]T. Zhang, C. N. Borca, X. Li, and S. T. Cundiff, Opt. Express **13**, 7432 (2005).
[48]U. Selig, F. Langhojer, F. Dimler, T. Lohrig, C. Schwarz, B. Gieseking, and T. Brixner, Opt. Lett. **33**, 2851 (2008).
[49]J. Helbing and P. Hamm, J. Opt. Soc. Am. B **28**, 171 (2011).
[50]D. B. Turner, K. W. Stone, K. Gundogdu, and K. A. Nelson, Rev. Sci. Instrum. **82**, 081301 (2011).
[51]J. A. Myers, K. L. Lewis, P. F. Tekavec, and J. P. Ogilvie, Opt. Express **16**, 17420 (2008).
[52]D. Brida, C. Manzoni, and G. Cerullo, Opt. Lett. **37**, 3027 (2012).
[53]D. Polli, L. Luer, and G. Cerullo, Rev. Sci. Instrum. **78**, 103108 (2007).
[54]S.-H. Shim and M. T. Zanni, Phys. Chem. Chem. Phys. **11**, 748–761 (2009).
[55]G. McDermott *et al.*, Nature **374**, 517 (1995).
[56]S. Niwa, L. J. Yu, K. Takeda, Y. Hirano, T. Kawakami, Z. Y. Wang-Otomo, and K. Miki, Nature **508**, 228 (2014).
[57]K. Nakagawa, S. Suzuki, R. Fujii, A. T. Gardiner, R. J. Cogdell, M. Nango, and H. Hashimoto, Photosynth. Res. **95**, 339 (2008).
[58]K. Nakagawa, S. Suzuki, R. Fujii, A. T. Gardiner, R. J. Cogdell, M. Nango, and H. Hashimoto, J. Phys. Chem. B **112**, 9467 (2008).
[59]J. Réhault, M. Maiuri, A. Oriana, and G. Cerullo, Rev. Sci. Instrum. **85**, 123107 (2014).
[60]J. Helbing and P. Hamm, J. Opt. Soc. Am. B **28**, 171 (2011).
[61]See supplementary material at http://dx.doi.org/10.1063/1.4919056 for a detailed description of the working principle of TWINS and for the fitted 2DES maps at different t2 delays.
[62]P. Bowlan, P. Gabolde, A. Shreenath, K. McGresham, and R. Trebino, Opt. Express **14**, 11892 (2006).
[63]I. H. M. van Stokkum, D. S. Larsen, and R. van Grondelle, Biochim. Biophys. Acta, Bioenerg. **1657**, 82 (2004).
[64]V. I. Novoderezhkin, R. Monshouwer, and R. van Grondelle, J. Phys. Chem. B **103**, 47 (1999).
[65]J. Hauer, M. Maiuri, D. Viola, V. Lukes, S. Henry, A. M. Carey, R. J. Cogdell, G. Cerullo, and D. Polli, J. Phys. Chem. A **117**, 6303 (2013).
[66]J. Knoester, J. Chem. Phys. **99**, 8466 (1993).